Temperature effect on water splitting using a Si-doped hematite photoanode

Paula Dias, Tânia Lopes, Luísa Andrade, Adélio Mendes*

LEPABE - Faculdade de Engenharia, Universidade do Porto, rua Dr. Roberto Frias,

4200-465 Porto, Portugal

Corresponding author: e-mail: mendes@fe.up.pt

Abstract

The influence of temperature on the performance of a photoelectrochemical (PEC) cell prepared with Si-doped hematite photoanode was studied for water splitting. The cell performance was characterized by photocurrent-voltage (*J-V*) characteristic curves and electrochemical impedance spectroscopy at different cell operating temperatures, from 25 ºC to 65 ºC. A standard three-electrode configuration comprehending the photoelectrode of hematite, the counter-electrode of pure platinum wire (99.9 %) and the reference electrode of Ag/AgCl/Sat.KCl was used. The identification of possible degradation pathways was addressed. It was observed that the generated photocurrent-density

increased with temperature. However, the photoelectrode became unstable above 50 ºC. The experiments performed concerning the study of the temperature effect and the aging showed that the optimal operation temperature of the PEC cell is ca. 45 ºC; this temperature ensures simultaneously the highest photocurrent-density and stability. This study is important for understanding the behavior of hematite photoelectrodes operating under real outdoor conditions.

1. Introduction

Nowadays, a particular interest in the development of promising technologies based on alternative and clean energy sources is emerging, especially motivated by the environmental awareness concerning fossil fuels dependence and for reducing the global warming effect.[1-3] An attractive strategy to turn over the actual energy problem is the use of solar radiation, the most abundant and sustainable renewable energy source. The variability of sunlight conditions arising from the night hours or the atmospheric and seasonal changes is one of the main challenges for the extensive use of energy from the Sun.[4, 5] A practical and potentially efficient route for storing solar power is to convert the solar radiation directly into chemical energy in the form of a fuel. Hydrogen is actually widely considered to be an environmentally friendly fuel of the future, when it is generated from renewable sources.[6] Photoelectrochemical (PEC) production of hydrogen under solar illumination is a promising renewable technology in the future hydrogen economy owing to the huge capacity of the solar energy. PEC cells use sunlight to split water into hydrogen (H_2) and oxygen (O_2) - photoelectrolysis.[7, 8] Fujishima and Honda first reported in 1972 the production of hydrogen via water splitting in a PEC cell using a photoanode of TiO_2 under UV illumination.[9] However, this technology only recently has received special attention from researchers.[10-14]

The working principles of a PEC cell based on a single photoelectrode and a metal counter-electrode are illustrated in the energy diagram of Fig. 1. This is the simplest possible configuration consisting of two electrodes: a photoactive semiconductor electrode and a platinum wire counter-electrode, both immersed in an electrolyte solution that allows the transport of the ionic species.[15, 16] The

photoelectrode (e.g. an n-type semiconductor photoanode immersed in an alkaline medium) absorbs photons with an energy that is equal to or larger than its bandgap to inject electrons from the valence to the conduction band and, consequently, creates electron-hole pairs. The electrons percolate through the external circuit and reach the counter-electrode surface to reduce water and subsequently generate H_2, while holes oxidize water to O_2 at the photoelectrode surface. Then, the cycle is closed when the electrolyte ions generated at the counter-electrode diffuse back to the surface of the semiconductor to recombine with holes.[6, 17]
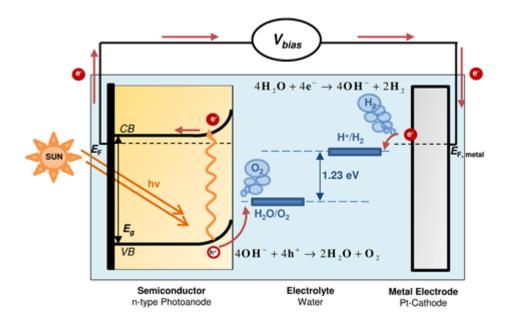

Fig. 1. Energy diagram of a PEC cell based on a photoanode and a metal counter-electrode in an alkaline medium.

The key component of PEC systems is the semiconductor photoelectrode. The ideal photoelectrode material for efficient solar hydrogen generation has to satisfy the following requirements: i) be made of a sufficiently abundant, safe and low cost material; ii) exhibit strong (visible) light absorption; iii) show efficient bulk

carrier separation and transport; iv) show efficient redox charge transfer surface reaction; and v) have long-term stability in the electrolyte.[6, 18] No semiconducting material with these properties has been found yet. This means that, so far, the development of PEC cells field is mainly focused on finding suitable photoelectrode materials to efficiently convert solar-to-hydrogen energy in a cost-effective way. Consequently, little efforts have been paid to study the performance of photoelectrochemical cells for water splitting under real conditions.

Photoelectrochemical cells for water splitting, as all other solar devices, are very sensitive to temperature. Two important works reporting the effect of temperature on photovoltaic parameters of solar cells were developed by Gupta *et al.* [19] and Sarswat *et al.* [20]. On Si-based solar cells, the temperature variations were intensively studied [21-24] and it was observed a decrease in the efficiency of the cell with temperature, mainly due to the decrease of the open-circuit voltage. According to the experimental investigations on several silicon cells, the output power decreases ca. 0.65 % per 1 K of temperature increase and the conversion efficiency decreases ca. 0.08 % K^{-1}.[25] For the organic solar cells, containing organic semiconductors such as polymer-fullerene [26], polyphenylene vinylene and copper phthalocyanine, the increase of temperature causes a monotonic increase of the short-circuit current (I_{sc}) and fill-factor (FF) and a linear decrease of the open-circuit voltage (V_{oc}).[27] The overall result is an increase of the energy conversion efficiency (η) at higher temperatures, reaching a maximum efficiency in the range of 47 ºC – 60 ºC.[28] Similar studies were developed for dye-sensitized solar cells (DSC).[29-31] Up to normal operation temperatures (45 ºC – 50 ºC) it is observed a slight gain in I_{sc} due to

more efficient electron diffusion on the TiO_2 film; on the other hand, at higher temperatures, the I_{sc} decreases due to an increased recombination rate.[32] The V_{oc} linearly decreases with temperature and, therefore, the energy efficiency dependence of the temperature is basically dominated by the I_{sc} and a maximum efficiency is reached for the normal operation temperatures.[33-35]

In what concerns the study of the temperature effect on PEC cells for water splitting, there are only few works. Recently, Andrade *et al.* [36] simulated the effect of outdoor conditions (temperature and solar radiation variations) on the energy performance of the PEC cells. A linear increase of the current-density with temperature was observed for undoped hematite photoanodes. Lopes *et al.* [37] studied the energy performance at 25 ºC and 35 ºC of a PEC cell constituted by a Si-doped hematite photoanode and an 8 % increase on the photocurrent-density at 1.45 V_{RHE} was observed.

Knowing the output performance of PEC cells as a function of temperature is especially important since electrode kinetics, catalytic activity, charge transfer, photoelectrode quantum efficiency, electrode stability, ionic mobility, diffusion and conductivity in the electrolyte significantly vary with temperature.[38] Understanding the behavior of these parameters gain special interest for outdoor applications since the cells are subjected to severe changes in temperature. The aging tests can also give essential information concerning the stability/corrosion of the overall photoelectrochemical system and, in particular, about the stability of the semiconductors. In PEC cells, stability issues is one of the major problem to be solved.[6] The stability of a semiconductor in contact with an electrolyte solution strongly depends on the competition between anodic dissolution and redox reaction, which are controlled by thermodynamic and kinetic parameters,

respectively.[39] Indeed, predicting the PEC cells performance as a function of the temperature and corresponding photoelectrode stability are crucial for the development of commercial devices.

In the present work, a PEC cell using a hematite photoanode was operated from 25 ºC to 65 ºC with steps of ca. 10 ºC. Characteristic J-V curves were obtained in the dark and under simulated sunlight (AM 1.5G, 1000 W m^{-2}). Electrochemical impedance spectroscopy (EIS) measurements were also performed in the dark. Aging tests were conducted at 3 different temperatures, 25 ºC, 45 ºC and 60 ºC, during 72 hours to analyze the stability of the PEC cell.

2. Theory

Two temperature effects on photoelectrochemical cells can be anticipated: thermal bandgap narrowing of the photoanode and decrease of potential required for electrolysis of water. Semiconductors are materials in which the range of excitation energies is interrupted by an energy bandgap of width E_g. In the case of photoanodes, which use n-type semiconductors, the valence band is nearly completely occupied with electrons and the conduction band is nearly empty. In order to excite an electron from the valence band to the conduction band by the absorption of a photon, it must equal at least the energy of the bandgap. This way, as temperature increases, the energy bandgap of a semiconductor reduces and the generated photocurrent tends to slightly increase since lower energy photons are also absorbed.[40] The dependence of the bandgap energy with temperature (T) is given by the Varshni model:[19]

$$E_g(T) = E_g(0) - \frac{\alpha' T^2}{T + \beta'}$$

(1)

where $E_g(0)$ is the bandgap of the semiconductor at 0 K, α' is the limit of the gap entropy when $T \to \infty$ and β' is expected to be comparable with the Debye temperature θ_D for a given material. A combination of a quadratic behavior, dominant in the low temperature range, with a linear behavior, dominant in the high temperature region, is expected.[19]

A semiconductor operating at lower temperatures will have fewer available free electrons and holes for charge transport. At the same time, heating exponentially increases the intrinsic carrier population, n_{int}, given by:[36]

$$n_{int}^2 \approx exp\left(-\frac{E_g}{k_B T}\right)$$

(2)

where k_B is the Boltzman constant. This effect is enhanced by the decrease of the bandgap at higher temperatures – Equation (1). Mass transport is also favored by an increased temperature as stated by the Einstein relation:[36]

$$D_i = \frac{k_B T}{q} \mu_i$$ (3)

where q is the elementary charge and μ_i is the mobility of species i.

However, increasing the temperature will also increase the current-density produced by the PEC cell, as described by the Butler-Volmer equation:[36]

$$j_{cell} = j_0 \left[\frac{n_{H_2O}(b)}{n_{H_2O}^{ref}(b)} exp\left(\frac{\beta n q \eta_{Pt}}{k_B T} \right) - \frac{n_{H_2}(b) n_{OH^-}^2(b)}{n_{H_2}^{ref}(b)\left(n_{OH^-}^{ref}\right)^2(b)} exp\left(\frac{-(1-\beta)n q \eta_{Pt}}{k_B T} \right) \right]$$ (4)

where j_0 is the exchange current density at the Pt counter-electrode, n_i is the density of the species i in the reaction, n^{ref} is the reference particle density, n is the number of electrons transferred in the reaction, q is the elementary charge and η_{Pt} is the overpotential at the platinum counter-electrode. The Butler-Volmer kinetics defines an exponential relation between the electric current crossing the electrolyte/platinum interface and the activation overpotential at the platinum cathode, where water is reduced to hydrogen gas with the consumption of two electrons, $n=2$ in Equation (4).

The temperature also influences the thermodynamics of a photoelectrochemical cell. The Nernst equation outlines how reversible electrochemical cell potential, E, varies as a function of species concentration and gas pressure:[41]

$$E = E^0 - \frac{RT}{nF} \ln\left(\frac{\Pi a_{i \, products}^{v_i}}{\Pi a_{i \, reactants}^{v_i}} \right)$$ (5)

where E^0 is the standard reversible voltage, R is the ideal gas constant, F is the Faraday constant, a_i are the activities (concentrations or gas pressures) of the reactant and product species and v_i are the stoichiometric coefficients. For accounting the temperature dependence, the Nernst equation should be modified:[41]

$$E = E^0 + \frac{\Delta s}{nF}\left(T - T_0\right) - \frac{RT}{nF}\ln\left(\frac{\Pi\, a^{v_i}_{products}}{\Pi\, a^{v_i}_{reactants}}\right) \tag{6}$$

where Δs is the standard entropy of the reaction (assumed to be temperature independent), T is the actual temperature of the system and T_0 is the ambient temperature. For the water splitting Equation (6) becomes:

$$E = E^0 + \frac{\Delta s}{nF}\left(T - T_0\right) - \frac{RT}{nF}\ln\left(\frac{a_{H_2}\, a^{1/2}_{O_2}}{a_{H_2O}}\right) \tag{7}$$

Since the entropy variation is negative, the electrolysis potential decreases with temperature.

The overall solar-to-hydrogen (STH) conversion efficiency, η_{STH}, is a critical property of a PEC cell. However, there is no agreement on the equation that should be used to obtain the PEC cell efficiency. According to the U.S. Department of Energy (DOE), the photoelectrochemical efficiency, η_{STH}, is defined as:[42]

$$\eta_{STH} = \frac{J_{ph} \times V_{redox} \times \eta_F}{P_{light}} \tag{8}$$

where J_{ph} is the generated photocurrent, V_{redox} is usually taken to be 1.23 V, based on a Gibbs free energy change for water splitting of 237 kJ mol^{-1}, η_F is the faradaic efficiency for hydrogen evolution and P_{light} is the incident sunlight (usually 1000 W m^{-2} with AM 1.5G). The faradaic efficiency for the hydrogen evolution and

oxygen evolution reactions is normally assumed to be unit, since the measured photocurrent corresponds to the molar generation of H_2, i.e. there are no parasite reactions.[42] Equation (8) describes the overall efficiency under zero bias conditions, which means that no external voltage is applied between the working electrode (WE) and counter-electrode (CE). When a bias is applied between the photo- and counter-electrodes, a new efficiency definition is needed, named "applied bias photon-to-current efficiency" (ABPE) [42]:

$$\eta_{ABPE} = \frac{J_{ph} \times \left(V_{redox} - \left| V_{bias} \right| \right)}{P_{light}}$$ (9)

where V_{bias} is the voltage applied to obtain the J_{ph}.[43] This definition, however, is meaningless since it does not tell the efficiency that should be assigned to the photonic conversion nor to the electrical conversion; aberrations such as obtaining null efficiency for a bias of 1.23 V, where the photoelectrochemical contribution is to overcome the overpotentials, are then possible. To overcome this limitation, the authors propose a set of new definitions for the efficiency to be used in PEC devices. The first definition concerns the overall PEC device efficiency (η_{device}), given by the ratio between the energy of the produced hydrogen and the total energy spent to accomplish the water splitting reaction, namely solar energy and external bias:

$$\eta_{device} = \frac{J_{ph} \times V_{redox}}{P_{light} + \left(J_{ph} \times V_{bias} \right)}$$ (10)

Equation (10) says nothing concerning the efficiency of the photoelectrodes. The efficiency of a photoanode should translate its ability to convert photonic energy into chemical energy used for oxidizing water. The energy needed to promote electrons coming from the anode to actually reduce water at the counter-

electrode - the external bias - must not enter into this definition. The proposed definition for the photoactive electrode efficiency is then:

$$\eta_{photoelectrode} \quad \frac{J_{ph} \times \left(V_{redox} - \left|V_{fb}\right|\right)}{P_{light}} \tag{11}$$

where V_{fb} is the flatband potential (note that this equation is valid either for photoanodes or photocathodes). The photoelectrode efficiency is then the energy of the produced hydrogen divided by the photonic energy supplied, assuming an external bias to provide the energy needed to bring the electron from the conduction band to the potential observed at the counter-electrode.

3. Experimental

In the present work, temperature influence on solar-to-hydrogen efficiency and stability of the PEC cells for water splitting was analyzed. Five temperatures were studied (25 ºC, 35 ºC, 45 ºC, 55 ºC and 65 ºC); a reference experiment at 25 ºC was performed between experiments in order to check the photoanode stability. The preparation of photoanode materials, the experimental test-bench and the PEC cell setup used to control the temperature, as well as the electrochemical measurements and the structural and morphological characterization of the PEC cells, are described in the following sections.

3.1.   Preparation of photoanode materials

Preparation of Si-doped α-Fe_2O_3 photoanodes

The mesoporous films of silicon-doped hematite were deposited on conducting fluorine-doped tin oxide (F:SnO_2) glass substrates by ultrasonic spray pyrolysis (USP) as described elsewhere.[44, 45] The substrates were first pretreated with tetraethoxysilane (TEOS) at ca. 400 ºC and were then hand-sprayed with approximately 3 mL per substrate of a diluted TEOS solution by using a glass atomizer. These samples were cooled down to the room temperature before being heated up again at 400 ºC to deposit the Fe_2O_3. To prepare the hematite films, a solution containing 20 mM iron(III) acetylacetonate (Fe(acac)$_3$) in EtOH with 1 wt. % TEOS as dopant was sprayed onto a temperature controlled substrate surface heated at 400 ºC with an ultrasonic spray nozzle from a distance of ca. 30 cm. A total of 60 sprays (one every 30 seconds) at a flowrate of 12 mL min^{-1} (spray length of 5 s) were performed, corresponding to a final film thickness of ca. 50 nm. A carrier gas flow (compressed air flow set to 15 L min^{-1})

directed the spray towards the substrates. After the spray, the samples were annealed for 30 min at ca. 500 ºC before cooling to room temperature.[44]

Preparation of electric contact on photoanodes

To prevent the contact of the electrolyte solution with the electric current collector of the photoanode and thus inducing corrosion, the current collector at the glass substrate of the photoanode was protected with an epoxy resin resistant to high temperatures. A conductive insulated wire was glued to the current collector using the epoxy resin.

3.2. Experimental test bench

When a photoelectrochemical cell is exposed to real atmospheric conditions, solar radiation and temperature are the two main factors that affect its performance. Thus, it is of great importance to know how a PEC cell behaves at different temperatures. An experimental test bench with a temperature controlling system was designed and built – Fig. 2.
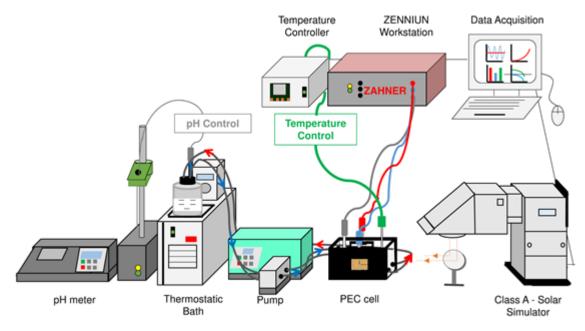
Fig. 2. Test bench for PEC cell characterization at different temperatures: (a) photo of the actual setup and (b) the corresponding scheme.

The electrolyte temperature was controlled using a water bath (Julabo, Germany) and the electrolyte was continuously pumped in and out of the PEC

cell by a recirculation system, as sketched in Fig. 2b. The pH of the electrolyte was controlled using a compact pH meter (WTW, Deutschland). For a more precise temperature control, a rubber heater (Omega Engineering Inc., US & Canada) was stuck to a stainless steel window, which was fixed against a window made of Teflon. These three new parts were screwed to a transparent acrylic part and screwed to the cell – Fig. 3. A Teflon coated thermocouple was placed inside the PEC cell contacting the electrolyte for reading the actual temperature; this temperature was used to control the rubber heater. The PEC cell configuration used is described elsewhere.[17, 46]
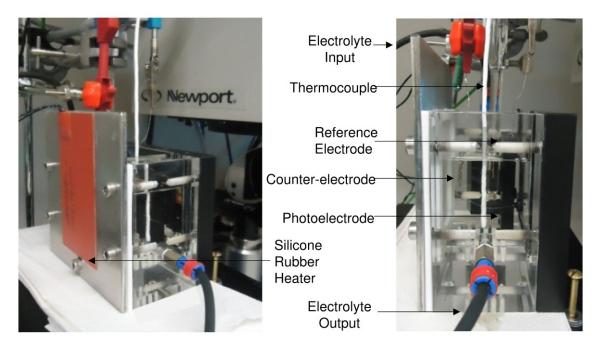

Fig. 3. Detail of the PEC cell equipped with a rubber heater for temperature controlled measurements.

A standard three-electrode configuration was used with the Si-doped α-Fe_2O_3 as photoanode, a 99.9 % pure platinum wire (Alfa Aesar, Germany) as counter-electrode and an Ag/AgCl/Sat.KCl (Metrohm, Switzerland) as a reference electrode. Thus, two sample holders are used: one keeps the semiconductor

vertically aligned and facing perpendicularly the light beam and the second one keeps the platinum wire aligned at the back of the sample. The distance between the holders is ca. 1 cm. The cell was filled with an electrolyte aqueous solution of 1.0 M KOH (25 ºC, pH 14), being its maximum volume of about 125 mL. The total immersed photoanode area was 4 cm^2.

3.3. J-V measurements

The photocurrent-photovoltage (*J-V*) characteristic curves were recorded applying an external potential bias to the cell and measuring the generated photocurrent using a ZENNIUM (Zahner Elektrik, Germany) workstation.[47] The measurements were performed in the dark and under simulated sunlight (Oriel solar simulator, 150 W Xe lamp, AM 1.5 G, ~1000 W m^{-2}) at a scan rate of 10 mV s^{-1} for the potential range between 0.6 V_{RHE} and 1.8 V_{RHE}. The light beam was calibrated with a c-Si photodiode.

3.4. EIS measurements

Electrochemical impedance spectroscopy (EIS) is a dynamic technique where a small potential sinusoidal perturbation is applied to the system and the amplitude and the phase shift of the resulting current response are recorded. EIS spectra were obtained also with the ZENNIUM workstation in dark conditions. The frequency range used was 1 Hz – 10 kHz and the magnitude of the modulation signal was 10 mV.[48] The measurements were performed at 0.8 V_{RHE}, 1.0 V_{RHE}, 1.2 V_{RHE} and 1.4 V_{RHE}. ZPlot/ZView® software (Scribner

Associates Inc.) was used to fit an appropriate electrical analog of the EIS spectra.

3.5. Aging tests

Aging tests consisted in applying a constant voltage to the PEC cell over several hours and measure the resulting time-dependent photocurrent response. The photocurrent history of the selected semiconductors provides important information about the stability/corrosion of the semiconductor. The measurements were performed at a constant applied potential of approximately 1.23 V_{RHE} during several hours and under constant irradiation conditions (AM 1.5 G, ~1000 W m^{-2}).

3.6. SEM characterization

Scanning electron microscope (SEM) was used to obtain information about morphology and surface topography of the photoelectrode materials. The morphology of the Si-doped hematite films was characterized using a high-resolution (50000× and 200000×) scanning electron microscope (FEI Quanta 400FEG). The acceleration voltage was 15 keV while an in-lens detector was employed with a working distance of about 10 mm. The surface of the samples was investigated before and after performing the photoelectrochemical measurements and after performing the aging tests to assess modifications in the surface morphology.

3.7. ICP technique

The inductively coupled plasma (ICP) technique is based on atomic spectrometry and offers extremely high accuracy and precision. In the present work, ICP-MS (Mass Spectroscopy) was used to quantify all elements with masses between 5 and 250 au present in the electrolyte solutions. ICP-AES (Atomic Emission Spectroscopy) was also used to determine more accurately the concentration of iron in the KOH electrolyte solutions. The electrolyte volume tested was ca. 50 cm^3.

4. Results and Discussion

4.1. J-V measurements

Fig. 4 shows the photocurrent density-voltage characteristic curves (*J-V*) of α-Fe$_2$O$_3$ photoanode doped with 5 % of silicon at five different temperatures, in the dark and under 1 sun AM 1.5G illumination. Before performing each *J-V* curve, the cell was left to stabilize for approximately 5 minutes.
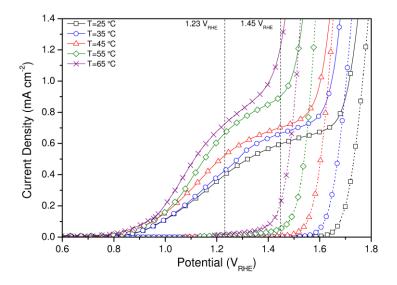

Fig. 4. Photocurrent density-voltage (*J-V*) characteristics of the Si-doped α-Fe$_2$O$_3$ electrode at various temperatures, in the dark (dashed lines) and under 1 sun simulated light (solid lines). (□) T=25 ºC, (○) T=35 ºC, (Δ) T=45 ºC, (◊) T=55 ºC, (×) T=65 ºC.

The performance of the cell increases with temperature – Fig. 4. At 25 ºC and under dark conditions, the current density rises steeply for a potential higher than 1.60 V$_{RHE}$ – the so-called dark current corresponding to the electrocatalytic water oxidation onset potential. Under sunlight conditions at 25 ºC, the photocurrent density is 0.40 mA cm^{-2} at the potential of reversible oxygen electrode (1.23

V_{RHE}), but it reaches a plateau only at approximately 1.45 V_{RHE} with a current of about 0.60 mA cm^{-2}. When the temperature of the electrolyte is increased to 35 ºC the dark current starts at approximately 1.55 V_{RHE}; the dark current starts earlier than for the experiment performed at 25 ºC. Under sunlight conditions the photocurrent density reaches 0.43 mA cm^{-2} at 1.23 V_{RHE}, corresponding to an increase of almost 8 %. Following the same analysis, a temperature increase of 40 ºC (sample characterized at 65 ºC) originates an 83 % enhancement of the photocurrent density at 1.23 V_{RHE}, but the dark current onset happens at 1.17 V_{RHE}.

Indeed, the photocurrent density of the PEC cell increases with temperature because the photoelectrode energy bandgap decreases and the charge transfer rate increases, cf. Equations (1)-(5). Moreover, the onset potential is shifted to lower potentials as the cell temperature increases, reducing the applied potential needed to initiate the water splitting reaction (bias). The influence of temperature on the energy conversion efficiency of the PEC cells is presented in Fig. 5.
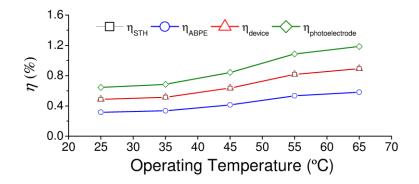

Fig. 5. Efficiency results obtained for the Si-doped α-Fe$_2$O$_3$ electrode as a function of the operating temperature: (□) solar-to-hydrogen efficiency, η_{STH}, (○) applied bias photon-to-current" efficiency, η_{ABPE}, (Δ) PEC device efficiency, η_{device}, (◊) photoanode efficiency, $\eta_{photoelectrode}$.

The efficiencies η_{STH}, η_{ABPE}, η_{device} and $\eta_{photoelectrode}$ were calculated using Equations (8), (9), (10) and (11), respectively. The faradaic efficiency in Equation (8) was assumed to be unit, since the measured photocurrent corresponds to the molar generation of H_2 without parasite reactions. For Equations (9), (10) and (11), the efficiencies were calculated for an external bias of 1.23 V_{RHE}. The incoming light considered was 1000 W m^{-2} and the flatband potential for the Si-doped α-Fe$_2$O$_3$ electrode was 0.40 V_{RHE}. The efficiency of the cell increases with temperature – cf. Fig. 5. However, the maximum current density is limited also by the onset potential of the dark current, which decreases with temperature; this effect should be also taken into account. Reference tests at 25 ºC performed between runs revealed possible degradation of the photoanode after running the PEC cell at 55 ºC and 65 ºC, since it resulted in changes in the *J-V* curves at 25 ºC (see Fig. S1 – Supporting Information). The best operating temperature of the PEC cell is therefore around 45 ºC, where the performance is the highest, acceptable dark current onset potential and no degradation was observed.

Fig. 6 shows SEM images of the Si-doped α-Fe$_2$O$_3$ tested sample, before and after performing the high-temperature tests. The sample area analyzed by SEM was made to coincide with the illuminated area during the different experiments. Actually, it was not noticed significant differences before and after running tests at 65 ºC. Thus, the shift on the dark current onset was not due to modifications on the hematite structure. The electrolyte solution used in these experiments was analyzed by ICP-AES and only trace amounts of Fe were found: 0.130 mg L^{-1}, 0.202 mg L^{-1} and 0.323 mg L^{-1} for tests performed at 25 ºC, 45 ºC and 65 ºC, respectively. Comparing the obtained values with the fresh solution (0.113 mg L^{-1}), a slightly increase was observed probably due to the smoothing of the

photoanode structure. However, the hematite sample did not suffer noticeable corrosion with the temperature tests as observed in Fig. 6, which may induce that this modification cannot be responsible for such significant left-shift of the dark current onset potential with temperature.
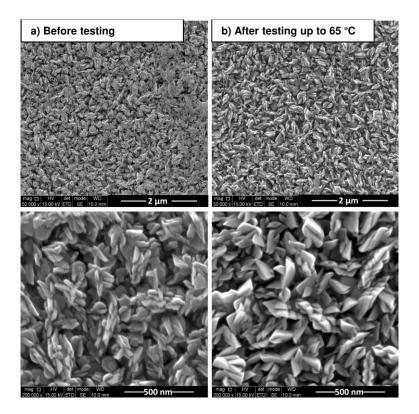

Fig. 6. SEM images of Si-doped α-Fe$_2$O$_3$: a) before and b) after performing the temperature tests until ca. 65 ºC with different resolution (top: 50000×; bottom: 200000×).

In order to pursue the comprehension of the such strong effect of temperature in the onset potential of the dark current, *J-V* curves of a bare transparent conductive oxide (TCO) glass substrate at 25 ºC, 35 ºC, 45 ºC, 55 ºC and 65 ºC were obtained – Fig. 7. The dark current of the bare TCO substrate starts at lower onset potentials values as temperature increases, behavior similar to the one

obtained for the hematite photoanodes (Fig. 4). The reference *J-V* curves at 25

ºC performed after each run shows that the TCO substrate is being progressively

damaged, which is more noticeable after performing the *J-V* curve at 55 ºC and

at 65 ºC (Fig. S2 - SI). This effect was also observed with the hematite

photoanodes. So, the shift on the dark current onset should be assigned to the

effect of temperature on the TCO-glass substrate and not due to changes in the

photoanode material as evidenced elsewhere.[49] The morphology of the TCO

substrates was studied using SEM – Fig. S3. After being used at high

temperatures (55 ºC and 65 ºC), the surface crystals of the TCO samples exhibit

a smother surface. Again the concentration of metals in the KOH electrolyte

solution used was analysed by ICP and the concentration of fluorine doubled in

the electrolyte used at 65 ºC, showing the possible degradation of the bare TCO

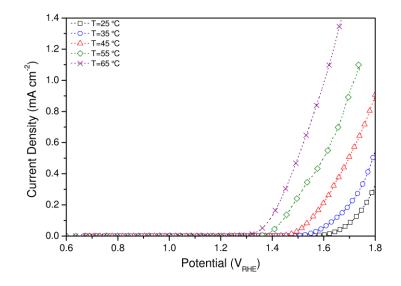made of fluorine doped tin oxide (FTO) (see Supporting Information – Table S1).

Fig. 7. Temperature effect in the photocurrent density-voltage (*J-V*)

characteristics of bare TCO substrate at a range of temperatures from 25 ºC to

65 ºC under the dark conditions. (□) T=25 ºC, (○) T=35 ºC, (Δ) T=45 ºC, (◊) T=55

ºC, (✕) T=65 ºC.

4.2. Aging tests

The stability of a PEC cell for water splitting is controlled by two factors: physical and chemical factors. Physical stability is related to electrolyte evaporation, which heats up under illumination. The chemical stability is associated to irreversible electrochemical and thermal degradation of the semiconductor and electrolyte.[50] The corrosion phenomena were investigated analyzing the content of iron in the electrolyte by ICP and the surface morphology of the photoelectrode by SEM. The measurements were performed at different temperatures (25 °C, 45 °C and 60 °C) under constant irradiation conditions (AM 1.5 G, ~1000 W m^{-2}), using an electrolyte solution of 1.0 M KOH and applying a constant bias potential of 1.23 V$_{RHE}$. The photocurrent-density history was performed only up to 60 °C, since a significant shift on dark current onset was observed at 55 °C and higher temperatures; this shift compromises the maximum current-density. Moreover, for higher temperatures the samples have no pratical application for water splitting. Fresh electrodes of Si-doped hematite with similar performances were used for each run, in a standard three-electrode configuration. The setup used is presented in Fig. 2.

Stability at 25 ºC

First, the stability performance was studied at 25 ºC during two periods of 72 hours. Between the two testing periods, the photoelectrode was submitted to a heating treatment in an oven (1.5 °C min^{-1} to 400 °C) [51] and the cell was filled with fresh electrolyte solution. Moreover, the sample was analyzed in terms of

photoelectrochemical performance by sweeping *J-V* scans in the dark and under simulated solar illumination. The corresponding *J-V* curves before and after running the two periods of stability tests are shown in Fig. 8 (left).
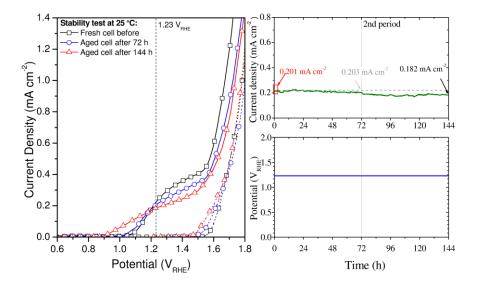

Fig. 8. Left: Photocurrent density-voltage (*J-V*) characteristics of the Si-doped α-Fe_2O_3 electrode tested in the dark (dashed lines) and under 1 sun simulated light at 25 °C (solid lines) before and after the stability test. (□) fresh cell before stability, (○) aged cell after 1st period of stability, (Δ) aged cell after 2nd period of stability. **Right:** Correspondent photocurrent history at a constant potential of 1.23 V_{RHE} and continuous 1 sun illumination at 25 °C.

The dark current density of the fresh hematite sample rises steeply for a potential higher than 1.55 V_{RHE}. Under simulated light conditions, the current density reaches a photocurrent value of about 0.22 mA cm^{-2} at 1.23 V_{RHE}. Photocurrent density-time dependent experiments are plotted in Fig. 8 (right) showing that the photocurrent density is acceptably stable over the time, with a performance decrease of ca. 9 % after 72 hours and ca. 22 % after 144 hours. This may indicate that some irreversible degradation occurs; however, the

photoanode did not exhibit signs of visual degradation. SEM characterization revealed that after the two periods of stability tests the grain structure of the hematite film becomes smother, cf. Fig. 9b vs Fig. 9a. Moreover, the iron concentration in the electrolyte solution was determined by ICP and it increased from 0.113 mg L^{-1} to 0.416 mg L^{-1}. Photocurrent values of 0.21 mA cm^{-2} and 0.19 mA cm^{-2} are obtained for aged cell after 72 hours and 144 hours under irradiated sunlight, respectively – Fig. 8. Moreover, the dark current rose for lower potentials, from 1.55 V_{RHE} to 1.45 V_{RHE} for the aged sample.
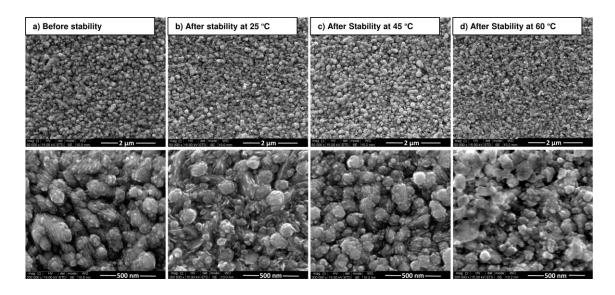

Fig. 9. SEM images of Si-doped α-Fe_2O_3 before (a) and after performing the stability tests with a constant potential of 1.23 V_{RHE} and continuous 1 sun illumination at three different temperatures: 25 °C (b), 45 °C (c) and 60 °C (d). (Top: 50000×; bottom: 200000×).

Stability at 45 °C

Fig. 10 (left) shows the *J-V* characteristics obtained before and after performing 72 h single period stability test at 45 °C. The photocurrent density for the fresh sample increases from of 0.20 mA cm^{-2} to 0.27 mA cm^{-2} at 1.23 V_{RHE},

respectively from 25 ºC to 45 ºC. After, the photocurrent density history was obtained for the temperature of 45 ºC – Fig. 10 (right). The photocurrent density is mostly stable over the first 60 hours with an average photocurrent value of 0.26 mA cm^{-2}. However, after 72 hours, a decay of 4 % in photocurrent was observed. No significant changes in the surface morphology of the sample were observed by SEM – Fig. 9c. The iron concentration in the electrolyte increased from 0.113 mg L^{-1} to 0.150 mg L^{-1} after the stability test.
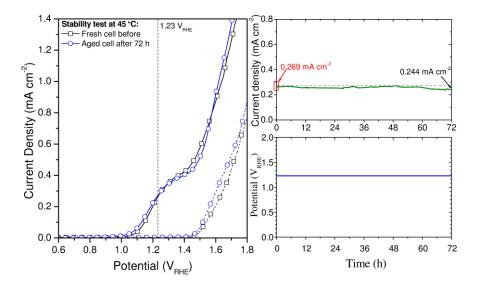

Fig. 10. Left: Photocurrent density-voltage (*J-V*) characteristics of the Si-doped α-Fe$_2$O$_3$ electrode tested in the dark (dashed lines) and under 1 sun simulated light at 45 ºC (solid lines) before and after stability. (□) fresh cell, (○) aged cell after 72 h of stability. **Right:** Correspondent photocurrent history at a constant potential of ~ 1.23 V$_{RHE}$ and continuous 1 sun illumination at 45 ºC.

Stability at 60 ºC

Fig.11 (left) shows the *J-V* curves at 25 ºC and 60 ºC, in the dark and under simulated solar illumination, before and after performing the 72 h stability test at

60 ºC. The fresh sample exhibited a photocurrent density of 0.18 mA cm^{-2} at 25 ºC and increased to 0.35 mA cm^{-2} at 60 ºC, for an external bias of 1.23 V$_{RHE}$. The current density of the photoelectrode at 60 ºC was mostly stable up to 30 h, decreasing afterwards to 0.19 mA cm^{-2} – Fig. 11 (right).

After the aging tests, the photoanode sample exhibited some visual signs of degradation in the illuminated area, suggesting that corrosion phenomena took place. SEM images of the fresh and aged hematite sample are shown in Fig. 8d. The aged sample exhibits a corroded surface with not well-defined grains and an overlapping structure of particles with smaller sizes. The electrolyte solution contained 1.130 mg L^{-1} of iron (electrolyte initial iron concentration was 0.113 mg L^{-1}), the highest value obtained for the studied electrodes.
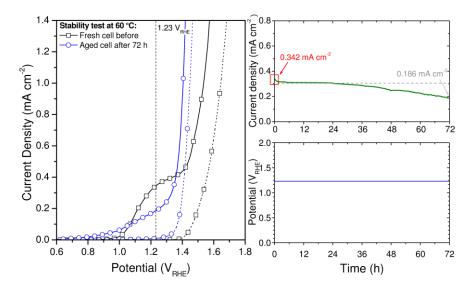

Fig. 11. Left: Photocurrent density-voltage (*J-V*) characteristics of the Si-doped α-Fe$_2$O$_3$ electrode tested in the dark (dashed lines) and under 1 sun simulated light at 60 ºC (solid lines) before and after stability. (□) fresh cell, (○) aged cell after 72 h of stability. **Right:** Correspondent photocurrent history at a constant potential of ~ 1.23 V$_{RHE}$ and continuous 1 sun illumination at 60 ºC.

4.3. EIS measurements

A three-electrode configuration was used to obtain information about the charge transfer kinetics at the semiconductor/electrolyte interface since the potential was measured with respect to a fixed reference potential, short-circuited with the counter-electrode.[52] The impedance spectra were obtained after performing the *J-V* characteristics of the hematite photoelectrode at the selected temperatures, i.e. from 25 ºC to 65 ºC with steps of 10 ºC. For each operating temperature, the charge transport resistances and the charge transfer at the interface of the photoelectrode/electrolyte of the PEC cell were obtained by fitting the EIS data to an electrical analogue – Fig. 12. Under dark conditions, the proposed electrical analogue considers a series resistance element, R_{Series}, and two RC elements in series: the first RC element models the electron transport in the semiconductor bulk, where R_{SC} is the semiconductor charge resistance and C_{SC} is the capacitance at the space charge layer on the semiconductor side; the second RC element represents the charge transfer resistance at semiconductor/electrolyte interface, where R_{CT} is the charge transfer resistance and C_H is the capacitance at the Helmholtz layer on the electrolyte side. The low-frequency response was assigned to the phenomena occurring in the semiconductor/electrolyte interface, whereas the high-frequency range was assigned to the faster electronic processes occurring in the semiconductor bulk. Moreover, in photoelectrodes formed by nanostructured semiconductors, the capacitance element is not ideal, showing a constant phase element (CPE) behavior.[16, 52, 53]
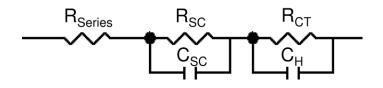
Fig. 12. Electrical circuit analogue used to fit the impedance data.

Fig. 13 shows the Nyquist plots obtained at an applied bias voltage of 0.8 V_{RHE}, 1.0 V_{RHE}, 1.2 V_{RHE} and 1.4 V_{RHE}, operating under dark conditions. The overall charge transfer resistance of the PEC system (R_{Series} + R_{SC} + R_{CT}) decreases with temperature for all applied potentials, explaining the overall increase of the photocurrent density with temperature. Two semicircles can be clearly distinguished (see inset of Fig. 13): one responding in the high frequencies range and the larger one responding in the low frequencies range. In fact, the low frequencies range semicircle decreases considerably with the temperature, being this decrease more obvious at higher temperatures (55 ºC and 65 ºC). Thus, the temperature increase strongly influences the phenomena occurring at the semiconductor/electrolyte interface.
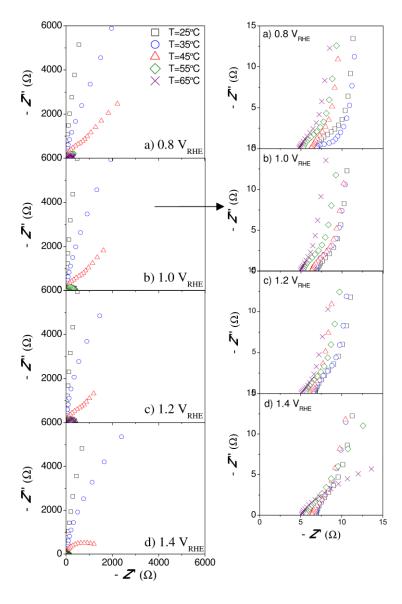
Fig. 13. Nyquist diagrams for a Si-doped α-Fe₂O₃ photoelectrode obtained in the dark at different temperatures and forward biases: 0.8 V$_{RHE}$ (a), 1.0 V$_{RHE}$ (b), 1.2 V$_{RHE}$ (c) and 1.4 V$_{RHE}$ (d). Z': real impedance, Z": imaginary impedance; (□) T=25 ºC, (○) T=35 C, (△) T=45 ºC, (◇) T=55 ºC, (✕) T=65 ºC. On the right side is a zoom-out of the left side plots.

Fig. 14 shows the impedance parameters for an applied potential of 1.2 V$_{RHE}$ as a function of the operating temperature. The potential of 1.2 V$_{RHE}$ was selected

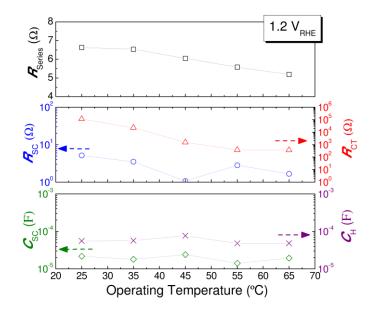since it is the closest potential to the reversible oxygen electrode potential (1.23 V_{RHE}).

Fig. 14. Impedance results obtained by fitting the experimental data shown in Fig. 13 for an applied potential of 1.2 V_{RHE} as a function of the operating temperature. (□) Series Resistance - R_{Series}, (○) Bulk Semiconductor Resistance – R_{SC}, (△) Charge Transfer Resistance – R_{CT}, (◊) Space Charge Capacitance - C_{SC}, (✕) Helmholtz Capacitance - C_H.

From Fig. 14 the series resistance, R_{Series}, decreases from 10.7 Ω to 6.2 Ω when temperature increases from 25 °C to 65 °C; this decrease is more pronounced at 55 °C and at 65 °C. R_{Series} comprises the TCO layer resistance and the external contacts resistance (e.g. wire connections); since the environment temperature around the external contacts did not change, the main contributor to R_{Series} is the TCO resistance.

The electrical resistance of the bulk semiconductor, R_{SC}, should decrease with temperature since faster electron transport is noticed [54, 55]; however, the highest decrease was observed at 45 °C with R_{SC} presenting 7.0×10^2 Ω - see Fig.

14. In fact, at around 60 °C the photoelectrode degrades with time, as observed from stability tests at 60 °C – Fig. 11. Thus, for temperatures above or equal to 55 °C the semiconductor matrix starts degrading, which should lead to stabilize the bulk resistance. Indeed, the behavior of the charge transport resistance in the bulk semiconductor with the temperature is the result of a balance between the photocurrent and the stability. Concerning the charge transfer resistance, R_{CT}, it decreases from 5.1×10^5 Ω to 2.7×10^3 Ω for the temperature range, also leveling out above 45 °C. The level out of the charge transfer resistance should be related to the degradation of the semiconductor that may be losing electrocatalytic activity. Indeed, it was found fluorine and tin in the electrolyte, probably resulting from the degradation of the TCO made of fluorine doped tin oxide (FTO) – see Supporting Information.

The capacitances values were also plotted as a function of the operating temperatures in Fig. 14. The Helmholtz capacitance (C_H) remains almost temperature independent (values in the order of magnitude of 10^{-4} F) and the space charge capacitance (C_{SC}) decreases with temperature. Though, a slightly increase for both capacitances is observed at 45 °C with 8.0×10^{-5} F and 2.6×10^{-4} F for C_{SC} and C_H, respectively. As R_{SC} decreases, the charge flow increases and, therefore, the thickness of the space charge layer decreases thereby justifying the C_{SC} increase at around 45 °C, since the capacitance is inversely proportional to the thickness of the layer. The C_H values are higher than the C_{SC} values, since the Helmholtz double layer width is generally smaller than the width of the depletion layer.[1, 3] This is the typical behavior of these capacitances for photo-assisted water splitting systems. Moreover, since the hematite semiconductor is doped with silicon, Si^{4+} acts as an electron donor improving its

electrical conductivity and, at the same time, reducing the width of the space charge layer that contributes to an increase of the C_{SC}.[14] In the case of heavily doped semiconductors, C_{SC} will be of the same order as C_H.[56]

Fig. 15 shows the Nyquist diagrams of three devices aged at different temperatures: 25 ºC (a), 45 ºC (b) and 60 ºC (c) and for an applied potential of 1.2 V_{RHE}. The first semicircle in the high frequency range, which is ascribed to the electron transfer process in the bulk semiconductor, is not clearly visible in the inset of Fig. 15. Though, the overall resistances tend to be smaller with time, being this behavior more evident as the temperature of stability test increases. After performing the stability test at 25 ºC, the sample did not reveal significant differences for the frequency range studied, even after 144 hours of testing - Fig. 15a. For the sample tested at 45 ºC during 72 h, the low-frequencies arc, assigned to the charge transfer in the semiconductor/electrolyte interface, becomes larger with the aging time, as shown in Fig. 15b. From Fig. 15c is visible different behaviors at the two frequency regions, which proves that a higher temperature (60 ºC) influences the stability of the electrode. Then, the impedance data was fitted to the electrical analog presented in Fig. 12 and the corresponding resistance and capacitance parameters were determined – Fig. 16.
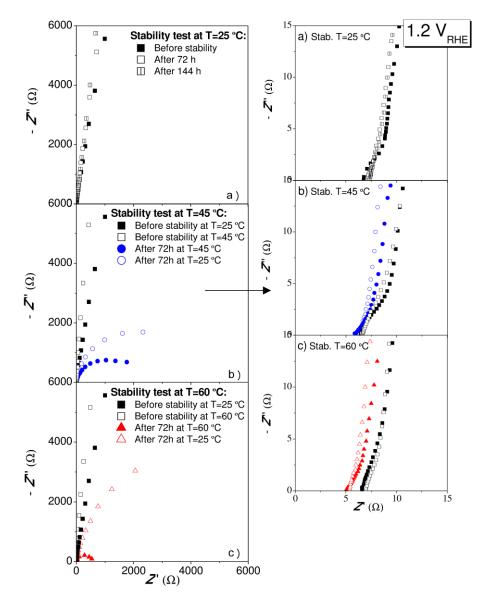
Fig. 15. Nyquist diagrams for a Si-doped α-Fe₂O₃ photoelectrode obtained in the dark with an applied potential of 1.2 V$_{RHE}$ at aged temperatures of 25 ºC (a), 45 ºC (b) and 60 ºC (c). Z ': real impedance; Z '': imaginary impedance.

Fig. 16 shows the resistances and capacitances obtained for fresh and aged samples. The series resistance slightly increases from 5.4 Ω to 6.0 Ω after 72 h of stability test, being the highest increase observed at 60 ºC. This series resistance change was assigned to the decrease of the TCO conductivity. Concerning the bulk semiconductor resistance, a significant variation from

4.2×10^2 Ω to 1.0×10^3 Ω was verified for the experiment performed at 60 ºC. This behavior is due to degradation of hematite photoanode with time – cf. Fig. 11. Similarly, the charge transfer resistance at the semiconductor/electrolyte interface increased with time and the major change was observed again at 60 ºC, since the deterioration of the semiconductor limits the charge transfer at the semiconductor/electrolyte interface. R_{CT} increased from around 3.0×10^3 Ω to 1.6×10^4 Ω after running 72 h of stability test at 60 ºC.

Finally, both C_{SC} and C_H are mostly constant during the stability tests at 25 ºC and 45 ºC. At 60 ºC the capacitances tend to decrease with aging time: C_{SC} decreased from 8.4×10^{-5} Ω to 4.3×10^{-5} Ω and C_H decreased from 1.9×10^{-5} Ω to 4.7×10^{-5} Ω, respectively. The hematite photoelectrode at 60 ºC showed surface corrosion, which should be related to the decrease of generated charges and further decrease of accumulated charges. These results confirm that 45 ºC is the highest temperature before the hematite photoelectrode start to corrode, simultaneously producing the highest photocurrent density.
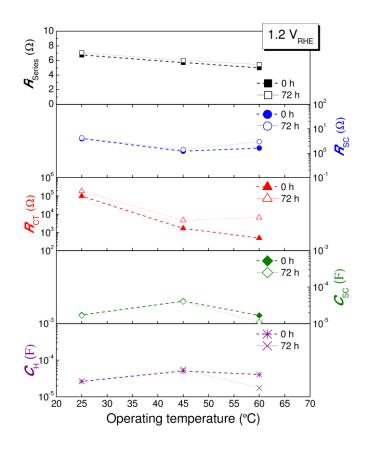
Fig. 16. Impedance results obtained by fitting the experimental data shown in Fig. 15 for an applied potential of 1.2 V$_{RHE}$ before (filled symbols) and after (open symbols) performing the stability tests during 72 h at three different temperatures: 25 ºC, 45 ºC and 65 ºC. (□) Series Resistance - R_{Series}, (○) Bulk Semiconductor Resistance – R_{SC}, (△) Charge Transfer Resistance – R_{CT}, (◊) Space Charge Capacitance - C_{SC}, (✕) Helmholtz Capacitance - C_{H}.

5. Conclusions

A study of the temperature effect on the performance of a photoelectrochemical cell for water splitting with hematite photoelectrodes was reported. *J-V* characteristic curves and EIS measurements were used to investigate the temperature- and time-induced changes in the PEC cells behavior. Understanding this behaviour is especially important for the development of commercial devices, since the cells are subjected to severe changes in temperature under outdoor applications. The PEC device composed by Si-doped α-Fe_2O_3 photoanodes in a standard three-electrode configuration was tested from 25 °C to 65 °C with steps of 10 °C. The results showed that the global performance of the PEC cell increases with temperature. A 33 % increase on the photocurrent density at 1.23 V_{RHE} was observed when the temperature was increased from 25 °C to 45 °C. On the other hand, an 83 % increase was obtained for the test temperature of 65 °C, but here the dark current onset starts at 1.17 V_{RHE}, before the potential of reversible oxygen electrode (1.23 V_{RHE}).

The effect of temperature on the dark current can be explained by the effect of temperature on TCO substrate, i.e. as temperature increases the onset potential tends to occur at lower potentials. Indeed, the very thin hematite layer employed allows the electrolyte to access to the TCO layer and this phenomenon increases with the operating temperature. The photocurrent-density history (stability tests) at different temperatures (25 °C, 45 °C and 60 °C) was obtained for fresh photoelectrodes during 72 h. Photoelectrode corrosion was observed at 60 °C and, as a consequence, the current density decreased 46 % after the aging period. The best operation conditions were obtained for 45 °C with improved energy performance and sufficient stability. The impedance analysis also

indicates that increasing the temperature makes the overall charge transfer resistance in the semiconductor/electrolyte interface of the cell to decrease. Additionally, the EIS spectra at 60 ºC for fresh and 72 h aged sample evidenced significant loss of activity.

Acknowledgment

References

[1] A.J. Nozik, Annual Review of Physical Chemistry, 29 (1978) 189-222.

[2] S.L. Nathan, in: C.I.o. Technology (Ed.) Report on the Basic Energy Sciences Workshop on Solar Energy Utilization, Renée M. Nault, 2005.

[3] A. Aruchamy, G. Aravamudan, G. Subba Rao, Bulletin of Materials Science, 4 (1982) 483-526.

[4] A. Valdes, J. Brillet, M. Gratzel, H. Gudmundsdottir, H.A. Hansen, H. Jonsson, P. Klupfel, G.-J. Kroes, F. Le Formal, I.C. Man, R.S. Martins, J.K. Norskov, J. Rossmeisl, K. Sivula, A. Vojvodic, M. Zach, Physical Chemistry Chemical Physics, 14 (2012).

[5] J. Nowotny, C.C. Sorrell, L.R. Sheppard, T. Bak, International Journal of Hydrogen Energy, 30 (2005) 521-544.

[6] R.V.d. Krol, Y. Liang, J. Schoonman, Journal of Materials Chemistry, 18 (2008) 2311-2320.

[7] M. Gratzel, Nature, 414 (2001) 338-344.

[8] L. Andrade, T. Lopes, H.A. Ribeiro, A. Mendes, International Journal of Hydrogen Energy, 36 (2011) 175-188.

[9] A. Fujishima, K. Honda, Nature, 238 (1972) 37-38.

[10] A. Kudo, Y. Miseki, Chemical Society Reviews, 38 (2009) 253-278.

[11] R. Abe, Journal of Photochemistry and Photobiology C: Photochemistry Reviews, 11 (2010) 179-209.

[12] M.G. Walter, E.L. Warren, J.R. McKone, S.W. Boettcher, Q. Mi, E.A. Santori, N.S. Lewis, Chemical Reviews, 110 (2010) 6446-6473.

[13] K. Sivula, F. Le Formal, M. Grätzel, ChemSusChem, 4 (2011) 432-449.

[14] I. Cesar, A. Kay, J.A. Gonzalez Martinez, M. Gratzel, Journal of the American Chemical Society, 128 (2006) 4582-4583.

[15] L.J. Minggu, W.R. Wan Daud, M.B. Kassim, International Journal of Hydrogen Energy, 35 (2010) 5233-5244.

[16] T. Lopes, L. Andrade, H.A. Ribeiro, A. Mendes, International Journal of Hydrogen Energy, 35 (2010) 11601-11608.

[17] T. Lopes, L. Andrade, A. Mendes, Photoelectrochemical Cells for Hydrogen Production from Solar Energy, in: N.E.A. Akbarzadeh (Ed.) Solar Energy Sciences and Engineering Applications, CRC Press, 2013.

[18] P.Z. Alan Kleiman-Shwarsctein, Yongsheng Hu, and Eric W. McFarlan, Solar Hydrogen Production by Photoelectrochemical Water Splitting: The Promise and Challenge, in: L. Vayssieres (Ed.) On Solar Hydrogen & Nanotechnology, John Wiley & Sons, Asia, 2010, pp. 704 pages.

[19] L. Gupta, S. Rath, S.C. Abbi, F.C. Jain, Pramana, 61 (2003) 729-737.

[20] P.K. Sarswat, M.L. Free, Physica B: Condensed Matter, 407 (2012) 108-111.

[21] E. Radziemska, E. Klugmann, Energy Conversion and Management, 43 (2002) 1889-1900.

[22] E. Radziemska, International Journal of Energy Research, 30 (2006) 127-134.

[23] P. Singh, S.N. Singh, M. Lal, M. Husain, Solar Energy Materials and Solar Cells, 92 (2008) 1611-1616.

[24] C. Wen, C. Fu, J. Tang, D. Liu, S. Hu, Z. Xing, SCIENCE CHINA Physics, Mechanics & Astronomy, 55 (2012) 235-241.

[25] E. Radziemska, Renewable Energy, 28 (2003) 1-12.

[26] B.C. Thompson, J.M.J. Fréchet, Angewandte Chemie International Edition, 47 (2008) 58-77.

[27] H. Hoppe, N.S. Sariciftci, Journal of Materials Research, 19 (2004) 1924-1945.

[28] I.E. Paulauskas, G.E. Jellison, L.A. Boatner, Journal of Materials Research, 25 (2010) 52-62.

[29] P.J. Sebastian, A. Olea, J. Campos, J.A. Toledo, S.A. Gamboa, Solar Energy Materials and Solar Cells, 81 (2004) 349-361.

[30] M. Berginc, U. Opara Krasovec, M. Jankovec, M. Topic, Solar Energy Materials and Solar Cells, 91 (2007) 821-828.

[31] H.J. Snaith, L. Schmidt-Mende, M. Grätzel, M. Chiesa, Physical Review B, 74 (2006) 045306.

[32] Z. Liu, S. Shen, L. Guo, International Journal of Hydrogen Energy, 37 (2012) 816-821.

[33] M. Berginc, U. Opara Krašovec, M. Hočevar, M. Topič, Thin Solid Films, 516 (2008) 7155-7159.

[34] M. Toivola, L. Peltokorpi, J. Halme, P. Lund, Solar Energy Materials and Solar Cells, 91 (2007) 1733-1742.

[35] S.R. Raga, F. Fabregat-Santiago, Physical Chemistry Chemical Physics, 15 (2013) 2328-2336.

[36] L. Andrade, T. Lopes, A. Mendes, Energy Procedia, 22 (2012) 23-34.

[37] T. Lopes, P. Dias, L. Andrade, A. Mendes, Energy Procedia, 22 (2012) 35-40.

[38] D.V. Esposito, O.Y. Goue, K.D. Dobson, B.E. McCandless, J.G.G. Chen, R.W. Birkmire, Rev. Sci. Instrum., 80 (2009).

[39] R. Memming, Semiconductor Electrochemistry, 1st ed., Wiley-VCH, 2001.

[40] J. Nelson, Analysis of the p-n Junction, in: The Physics of Solar Cells, Imperial College Press, 2003, pp. 145-176.

[41] R. O'Hayre, S.-W. Cha, W. Colella, F.B. Prinz, Fuel cell fundamentals, John Wiley & Sons, New York, 2006.

[42] Z. Chen, T.F. Jaramillo, T.G. Deutsch, A. Kleiman-Shwarsctein, A.J. Forman, N. Gaillard, R. Garland, K. Takanabe, C. Heske, M. Sunkara, E.W. McFarland, K. Domen, E.L. Miller, J.A. Turner, H.N. Dinh, J. Mater. Res., 25 (2010) 3.

[43] R. Krol, Introduction, in: R. van de Krol, M. Grätzel (Eds.), Springer US, 2012, pp. 3-12.

[44] F.L. Formal, M. Grätzel, K. Sivula, Advanced Functional Materials, 20 (2010) 1099-1107.

[45] A. Duret, M. Gratzel, The Journal of Physical Chemistry B, 109 (2005) 17184-17191.

[46] T. Lopes, P. Dias, L. Andrade, A. Mendes, Solar Energy Materials and Solar Cells, 128 (2014) 399-410.

[47] Zahner, in, 2009.

[48] H. Dotan, K. Sivula, M. Gratzel, A. Rothschild, S.C. Warren, Energy & Environmental Science, 4 (2011) 958-964.

[49] P. Dias, T. Lopes, L. Andrade, A. Mendes, Under Submission (2014).

[50] A. Hinsch, J.M. Kroon, R. Kern, I. Uhlendorf, J. Holzbock, A. Meyer, J. Ferber, Progress in Photovoltaics: Research and Applications, 9 (2001) 425-438.

[51] K. Sivula, R. Zboril, F. Le Formal, R. Robert, A. Weidenkaff, J. Tucek, J. Frydrych, M. Grätzel, Journal of the American Chemical Society, 132 (2010) 7436-7444.

[52] T. Lopes, Andrade, L., and Mendes, A., Photoelectrochemical Cells for Hydrogen Production from Solar Energy in Solar Energy Sciences and Engineering Applications, in: A.A. Napoleon Enteria (Ed.) Solar Energy Sciences and Engineering Applications, CRC Press Taylor & Francis Group, 2013, pp. 692.

[53] T. Lopes, L. Andrade, F. Le Formal, M. Gratzel, K. Sivula, A. Mendes, Physical Chemistry Chemical Physics, (2014).

[54] Q. Wang, S. Ito, M. Grätzel, F. Fabregat-Santiago, I. Mora-Seró, J. Bisquert, T. Bessho, H. Imai, The Journal of Physical Chemistry B, 110 (2006) 25210-25221.

[55] N. Lu, A. Ji, Z. Cao, Sci. Rep., 3 (2013) 3090.

[56] F. Le Formal, N. Tetreault, M. Cornuz, T. Moehl, M. Gratzel, K. Sivula, Chemical Science, 2 (2011).